

## On the Formation of 50?nm Diameter Free-Standing Silicon Wires Produced by Ion Irradiation

J. Song, Z. Y. Dang, S. Azimi, M. B. H. Breese, J. Forneris and E. Vittone

*ECS J. Solid State Sci. Technol.* 2012, Volume 1, Issue 2, Pages P66-P69.

doi: 10.1149/2.015202jss

---

**Email alerting  
service**

Receive free email alerts when new articles cite this article - sign up in the box at the top right corner of the article or [click here](#)

---

---

To subscribe to *ECS Journal of Solid State Science and Technology* go to:  
<http://jss.ecsdl.org/subscriptions>

---

© 2012 The Electrochemical Society



## On the Formation of 50 nm Diameter Free-Standing Silicon Wires Produced by Ion Irradiation

J. Song,<sup>a</sup> Z. Y. Dang,<sup>a</sup> S. Azimi,<sup>a,\*</sup> M. B. H. Breese,<sup>a,b,z</sup> J. Forneris,<sup>c</sup> and E. Vittone<sup>c</sup>

<sup>a</sup>Centre for Ion Beam Applications (CIBA), Department of Physics, National University of Singapore, Singapore 117542

<sup>b</sup>Singapore Synchrotron Light Source (SSLS), National University of Singapore, Singapore 117603

<sup>c</sup>Experimental Physics Department and NIS Excellence Centre, University of Torino, 10125 Torino, Italy

Ion irradiation in conjunction with electrochemical etching is a promising silicon (Si) machining technique for three-dimensional nanofabrication. We present a study of factors influencing the formation of silicon nanowires fabricated by this technique, such as ion energy, fluence, proximity of adjacent wires, location within an irradiated area and wafer resistivity. A better understanding of these factors in different resistivity wafers has enabled us to produce wire diameters and gaps between adjacent wires of about 50 nm using 50 keV protons. Multilayer silicon nanowire arrays are also achieved, so extending the use of this process for three dimensional nanoscale silicon machining.

© 2012 The Electrochemical Society. [DOI: 10.1149/2.015202jss] All rights reserved.

Manuscript submitted April 23, 2012; revised manuscript received May 24, 2012. Published July 20, 2012.

A micromachining process using high-energy, light ions to irradiate p-type silicon, which is then electrochemically etched in dilute hydrofluoric acid has been developed.<sup>1-3</sup> This process has been used to fabricate a range of patterned microstructures in porous silicon and other semiconductors.<sup>4-7</sup> The defect density in silicon produced by ion irradiation depends on many factors; defects can be stable or they may agglomerate into more stable divacancies and other vacancy or impurity-related centers.<sup>8-10</sup> Many types of defects act as trap levels where charge carriers undergo recombination, so reducing the hole density and increasing the resistivity<sup>11</sup> along the ion trajectories. Ion irradiation typically thus reduces the electrical hole current flowing through such regions of p-type silicon during subsequent electrochemical etching,<sup>12</sup> slowing down or completely stopping etching, leaving unetched regions, while in other etched regions porous silicon will be formed.<sup>2,3</sup>

The defect production rate of light ions, such as protons and helium ions, with energies greater than about 50 keV peaks close to the end of their range.<sup>13,14</sup> At a low fluence, only the end-of-range region remains unetched, while the regions above and below it are etched, resulting in a buried silicon core surrounded by porous silicon. If we irradiate a line on the surface of a silicon wafer, a wire will be formed at the end-of-range region. This approach has been used to fabricate multimode waveguides<sup>6,15</sup> and to create three-dimensional patterned surfaces<sup>16</sup> and arbitrary shaped three-dimensional structures.<sup>17</sup> However, to fabricate single mode silicon waveguides, wire diameters of 300 to 400 nm are required,<sup>18</sup> which were not previously achieved by this approach. Furthermore, the inability to use high-energy, high fluence ion irradiation followed by electrochemical etching for etching gaps smaller than 2  $\mu\text{m}$  between irradiated lines was previously discussed.<sup>3</sup> This limited further application of this micromachining approach in fields such as silicon photonics since it precluded the ability to couple near infra-red light between adjacent waveguides, or into resonator structures, both of which require gaps of the order of a hundred nanometers or less.

The main motivation for this study is to address the lack of understanding of the relationship between the achievable wire diameter and gap between adjacent wires as a function of ion energy, fluence, beam size and wafer resistivity in order to extend this process to fabricating nanoscale wires in silicon. We use 50 keV proton irradiation of p-type silicon of two wafers over a range of resistivity, from  $\rho = 0.02 \Omega \cdot \text{cm}$  (doping density  $N_A = 4.8 \times 10^{18} / \text{cm}^3$ ), to  $0.4 \Omega \cdot \text{cm}$  ( $N_A = 4.8 \times 10^{16} / \text{cm}^3$ ). Lower resistivity wafers are ideal for machining different surface topography, such as patterned distributed Bragg reflectors,<sup>7</sup> concave micromirrors and holographic surfaces, since the etch rate is inversely proportional to the fluence.<sup>2,7</sup> Higher resistivity

wafers are more suitable in silicon photonics where the lower doping density gives lower scattering losses from free carriers.<sup>18</sup>

### Definition of Line Fluence

The standard unit to quantify the number of ions used for irradiation is the fluence, defined as the number of ions incident upon a given surface area, in units of ions/cm<sup>2</sup>. This definition is ideal for irradiating large areas where the effects of irradiation are laterally uniform and the defect depth distribution may be calculated using codes such as SRIM 2011 (Stopping and Range of Ions in Matter). If the irradiated surface line width is similar to or smaller than the size of ion lateral straggling effect at the end-of-range, the average defect density within the end-of-range region decreases compared to that for an irradiated large area, for a fixed fluence. From SRIM simulations for a proton beam energy of 50 keV the defect density starts to drop for line widths of less than 200 nm, so the definition of fluence is not adequate for describing the relationship between irradiated line widths of 90 nm used in this work and the resultant wire diameter formed at the end of range. A more useful parameter is the *line fluence*, given by the number of ions used for irradiating a line of zero width per centimeter of line length. This definition is independent of the irradiated line width on the surface and it simplifies the experimental aspects of fabricating small wires since the only parameters are the total number of ions used, their energy and type.

### Experimental

Larger scattering at higher proton energies results in defects distributed over a larger lateral distance away from the beam axis. Therefore, to fabricate small diameter wires, a low proton energy seems preferable, also requiring a lower fluence to achieve a given peak defect density compared to higher energy irradiation. We study the effect of proton energy by comparing wire diameters obtained using 50 and 250 keV proton irradiation, with all other factors kept the same. For irradiating lines with energies above 250 keV, direct writing using a nuclear microprobe can be used, but for lower energies direct writing is not suitable as beam transmission through the accelerator is low and focusing becomes more difficult. For proton irradiation at 50 keV energy, we used electron beam lithography to first pattern a 1000 nm thick PMMA (polymethyl methacrylate) layer with line widths of 90 nm. Resist-coated wafers were then irradiated using our accelerator operating at a terminal voltage of 100 kV, giving 100 keV molecular hydrogen ions, H<sub>2</sub><sup>+</sup>, using our large area irradiation facility,<sup>19</sup> which ensures uniform irradiation, with no undesirable variations in fluence produced by any beam current fluctuations. When H<sub>2</sub><sup>+</sup> ions impact on the surface, they break into two 50 keV protons, which have a range of about 470 nm in silicon and 820 nm in PMMA. The PMMA layer is therefore thick enough to stop 50 keV protons, so the only wafer

\*Electrochemical Society Student Member.

<sup>z</sup>E-mail: phymbhb@nus.edu.sg

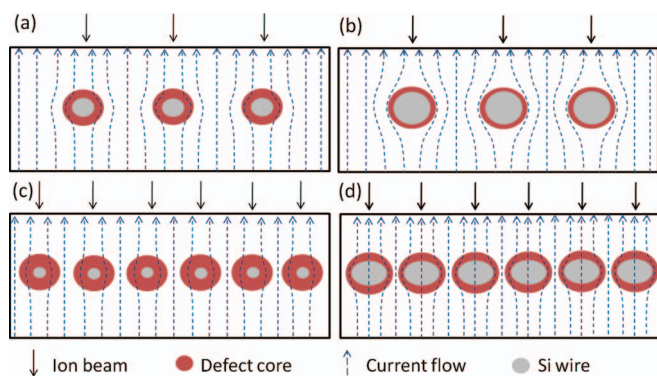


**Figure 1.** (Color online) Schematic of wire formation process during electrochemical etching for (a) (c) low line fluence and (b) (d) high line fluence.

portions irradiated are through the 90 nm wide exposed areas. Electrochemical etching is performed using a dilute electrolyte of HF (48%): ethanol in the ratio of 1:1, with a current density of  $40 \text{ mA/cm}^2$  for  $0.4 \Omega \cdot \text{cm}$  wafer and  $60 \text{ mA/cm}^2$  for  $0.02 \Omega \cdot \text{cm}$  wafer and an etching time of 1 to 4 minutes. To prepare samples for cross-section scanning electron microscopy (SEM), line lengths of several hundred microns were irradiated and the wafer was cleaved after etching.

### Single Energy Ion Irradiation

The schematic in Fig. 1 summarizes the process and observed dependence of resultant wire diameter on line fluence and spacing in this work. Irradiation produces a high defect density within the end-of-range core. During subsequent electrochemical etching the hole current flow is deflected away from this region resulting in wire formation. For the widely separated line irradiations in Fig. 1a, 1b a higher line fluence increases the size of the end of range region over which the core resistivity is increased, causing the etch current to bend further round it, producing a larger wire diameter. This behavior is observed in Figure 2 which shows wires formed for increasing line fluence in  $0.4 \Omega \cdot \text{cm}$  wafers, for a line period of  $2 \mu\text{m}$ , large enough such that they undergo etching as isolated wires and not influenced by proximity to other line irradiations. The resultant wire diameter increases from 100 to 360 nm over this range of line fluences.

Figure 3a compares the measured diameter of isolated wires produced with 250 and 50 keV protons in both wafer resistivities. A higher line fluence is typically required for wire formation at higher

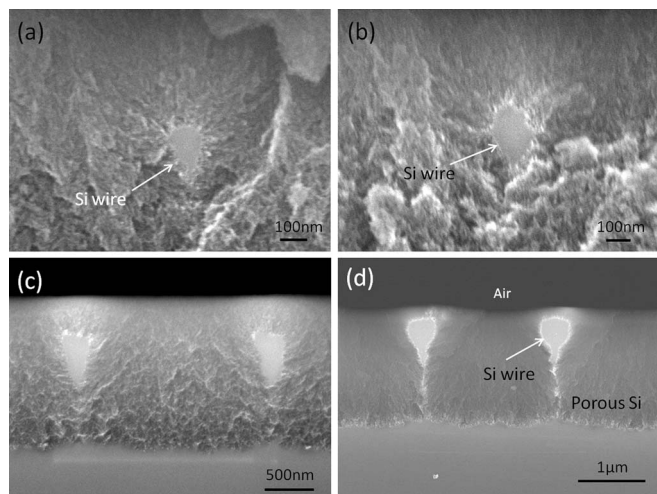


**Figure 2.** Cross-section SEMs of individual wires for 50 keV proton line fluences of (a)  $9 \times 10^8/\text{cm}$ , (b)  $1.3 \times 10^9/\text{cm}$ , (c)  $1.8 \times 10^9/\text{cm}$ , (d)  $3.2 \times 10^9/\text{cm}$ .

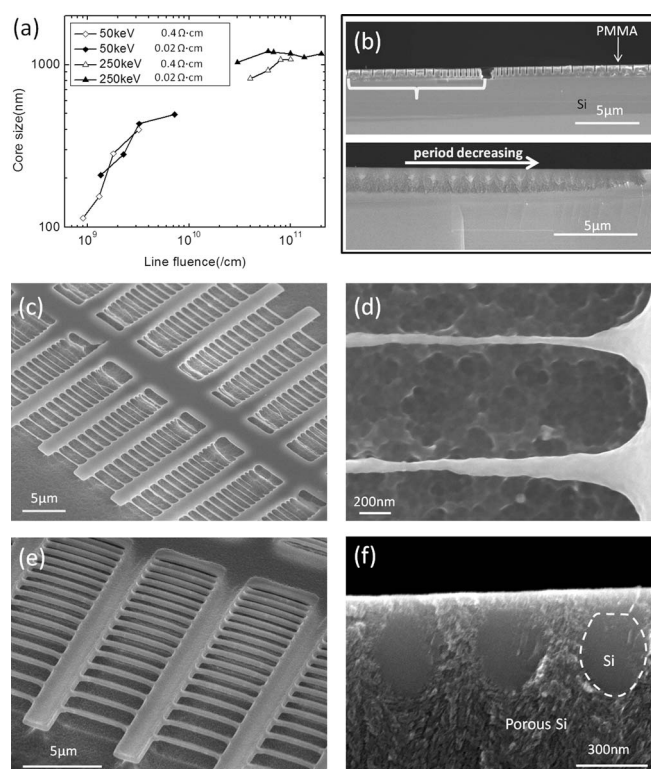


**Figure 3.** (a) Plot of wire diameter versus line fluence for two proton energies and two wafer resistivities. (b) upper: cross-section SEM of 1000 nm thick E-beam patterned PMMA resist. lower: resultant etched  $0.4 \Omega \cdot \text{cm}$  wafer using a line fluence of  $1.3 \times 10^9/\text{cm}$ , showing the direction of decreasing line spacing. (c), (d) plan view SEMs of the freestanding wires in a  $0.4 \Omega \cdot \text{cm}$  wafer after porous silicon removal for line fluences of  $2.2 \times 10^9/\text{cm}$  and  $1.3 \times 10^9/\text{cm}$  respectively. (e) plan view SEM of structure produced in a  $0.02 \Omega \cdot \text{cm}$  wafer after porous silicon removed for a line fluence of  $2.2 \times 10^9/\text{cm}$ . (f) cross-section SEM of individual wires before porous silicon removal. The profile of the right-most wire is shown in a dashed, white line.

energies owing to a reduced defect density within the wire. For a given energy the lateral size of wires are similar in both wafers, increasing with line fluence. From this we conclude that the wire sizes are largely determined by the extent of the ion induced defect distribution.

Figure 3a shows results for isolated wires only. To study the effect of the proximity of adjacent wires and wire location within an irradiated region, arrays of lines were irradiated using 50 keV protons with a uniform line fluence. In some structures the period between adjacent lines decreased from the outer edges toward the center of the irradiated pattern. In other structures the line period was fixed.

Figure 3b shows a cross-section SEM of the corresponding electron beam irradiated polymer resist, where the direction of decreasing period from  $1.5 \mu\text{m}$  down to  $300 \text{ nm}$  between irradiated lines is indicated. Figure 3b shows a higher magnification cross-section SEM of the resultant wires after irradiating a  $0.4 \Omega \cdot \text{cm}$  wafer with a 50 keV proton line fluence of  $1.3 \times 10^9/\text{cm}$ . This line fluence results in an isolated wire diameter of  $\sim 150 \text{ nm}$  in Fig. 3a, but in Fig. 3b the wires vary in diameter even though the line fluence is constant; this observation is important to the understanding of what minimum wire diameter may be achieved for a given line fluence in a densely-machined structure. Wire diameters of  $\sim 150 \text{ nm}$  are produced at the outer edges of the irradiated region, but decrease in size toward the center and disappear totally for line periods less than  $700 \text{ nm}$ , where the etch rate starts to reduce, as deduced by the silicon/porous silicon interface becoming shallower. We interpret this observation as follows: as the wires become closer together the etch current is forced to flow close to, or even through the wires, resulting in them being progressively etched away, as seen by comparing Fig. 1a, 1c. This emphasizes the importance of

the location of a feature within an irradiated area in determining its final size, not just the line fluence.

Other  $0.4 \Omega \cdot \text{cm}$  wafers were similarly patterned with a polymer resist, with the addition of  $2 \mu\text{m}$  wide irradiated lines running perpendicular to the narrow lines to provide a support structure. After irradiation and etching, the  $2 \mu\text{m}$  lines are not undercut, so remain attached to the substrate and the wires are attached to them. Figures 3c, 3d show plan view SEMs of such structures with the porous silicon removed. For such narrow wires as observed here the usual removal process with dilute KOH destroys the lines due to the large bubbling involved. Instead, first the porous silicon was oxidized and then removed using dilute HF, which involves little bubbling. This enabled removal of the porous silicon and observation of the remaining wires as freestanding nanoscale wires without being destroyed. Figure 3d shows a higher magnification SEM of lines irradiated with  $1.3 \times 10^9/\text{cm}$  and an line period of 850 nm, chosen as being just larger than that where the wires disappear in Fig. 3b. This results in wires with diameters varying from 40 to 60 nm, compared with  $\sim 150$  nm for isolated wires under the same conditions. The wire width produced by this method typically varies by  $\pm 10$  nm in diameter over lengths of hundreds of nanometers and AFM (atomic force microscope) measurements of a  $1.5 \times 1.5 \mu\text{m}^2$  area of the wire support in Fig. 3c show a surface roughness of 7 nm. The relatively high roughness is attributed to the use of a moderately high wafer resistivity which results in a rougher surface than lower resistivities,<sup>20,21</sup> rather than to variations in line fluence along the wire, which are small.<sup>19</sup> We have shown on other similar wires that both the roughness and variations in diameter are greatly reduced after high temperature oxidation.<sup>22</sup> While wires as small as  $\sim 50$  nm can be fabricated in the  $0.4 \Omega \cdot \text{cm}$  wafer using 50 keV protons, the achievable minimum gap between them remains large, at about  $\sim 600$  nm, similar to that produced using higher proton energies of 250 keV (not shown here).

A similar array of freestanding wires was fabricated in the  $0.02 \Omega \cdot \text{cm}$  wafer, shown in Fig. 3e. Figure 3f shows a higher magnification cross-section SEM of a similar structure irradiated with the same line fluence and a line period of 450 nm with the porous silicon still present. A wire diameter of  $\sim 270$  nm is achieved, similar to that produced for isolated wires for the same fluence (Fig. 3a), so clearly the less resistive wafer is less affected by proximity to adjacent wires than the  $0.4 \Omega \cdot \text{cm}$  wafer. The smaller line period results in a gap of only  $\sim 180$  nm. Clearly, much smaller gaps may be produced in lower resistivity p-type silicon, which we attribute to a smaller lateral deflection of the etch current produced by a smaller perturbation of the electrostatic potential within the more highly-doped material.

Figure 4 shows cross-section SEMs of arrays of wires where a different approach is taken to fabricating very small gaps. Larger line periods and higher line fluences were used to make the resultant wires large enough so that they are not fully dissolved away by the passage of etch current through them at small gap sizes, Fig. 1c, 1d. The flattening of the upper wire surface is because the component of current which flows through the wire causes the upper surface to be etched away. As the period is reduced from 650 nm to 550 nm, for a fixed line fluence, the gap size reduces, Fig. 1b, 1d. As the line fluence is increased, for a fixed period, the gap size also reduces, Fig. 1a, 1b, so producing a very small gap is just a question of finding the best combination between these two parameters. Gaps of about 50 nm are circled in Fig. 4c. For a period of 550 nm, on increasing the line fluence the vertical size of the wire reduces, again due to the flow of current forced through the small gap, resulting in more flowing through the silicon wire region, so producing a thinner wire. This effect is not observed for the 650 nm line period, as this does not result in such small gaps.

### Multiple Energy Ion Irradiation

The above process can be extended to three dimensional (3D) wire fabrication using the different depth of the end-of-range wires produced by different beam energies. Fig. 5 shows a schematic of the process of multiple energy ion irradiation. Electron beam lithography is used to pattern a 1000 nm thick PMMA layer on top of  $0.02 \Omega \cdot \text{cm}$

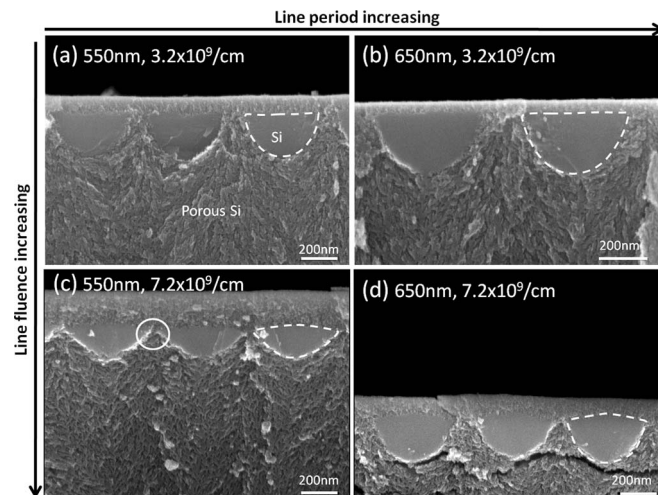


**Figure 4.** Cross-section SEMs of individual wires in  $0.02 \Omega \cdot \text{cm}$  wafers irradiated with 50 keV protons with varying period and line fluence. The right-most wire profile is highlighted with a dashed white line in each case and the white circle indicates a 50 nm gap area.

silicon wafer with line width of 200 nm and period of  $1.2 \mu\text{m}$ . The resist-coated wafer is then irradiated by 50 keV and 250 keV proton beam. The PMMA resist is thick enough to stop the 50 keV proton beam so only the exposed parts are irradiated, resulting in an end-of-range core region at  $\sim 470$  nm beneath the surface. The 250 keV proton beam penetrates the PMMA, resulting in a core region at  $1.7 \mu\text{m}$  beneath the wafer surface which is covered with PMMA whereas at the exposed surfaces the core region is located at a depth of  $2.4 \mu\text{m}$ . This results in three layers of cores, which, after etching, produces a multi-level wire array. Figure 6 shows cross-section SEMs of such a multilevel structure. This process is best suited to the lower resistivity wafer in which it was shown above that smaller gaps could be formed. This is important for extending this process to a 3D geometry where the etch current has to flow between narrow gaps both laterally and vertically. The fluence used for the higher energy irradiation must be larger than that of low energy beam to properly form

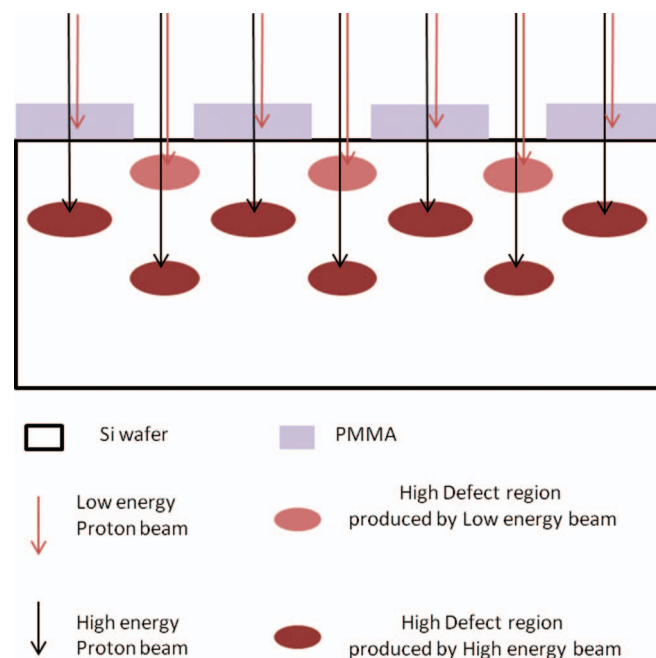


**Figure 5.** (color online) Schematic of multiple energy ion irradiation.

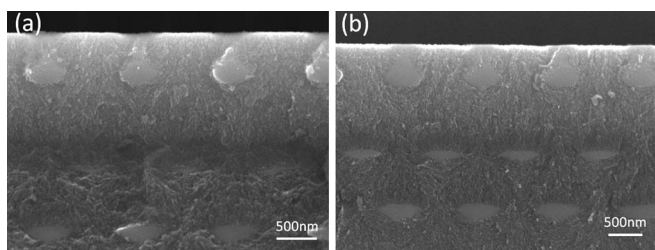


**Figure 6.** Cross-section SEMs of three dimensional silicon nanowire arrays in  $0.02 \Omega \cdot \text{cm}$  wafers irradiated with 50 keV protons with line fluence of (a)  $5.6 \times 10^9/\text{cm}$  (b)  $7 \times 10^9/\text{cm}$ , and 250 keV protons with line fluence of (a)  $1 \times 10^{10}/\text{cm}$  (b)  $1.8 \times 10^{10}/\text{cm}$  according to the 200 nm exposed area.

wires. Comparing Fig. 6a, 6b we note that the formation of the middle row of wires is more sensitive to the high energy beam fluence than the lower row. This is because the etch current which is deflected around the wires in the lowest row produces a larger etch current directed toward the cores within the middle layer, making them more sensitive to variations in wire size. This again highlights the importance of the location of a core within an irradiation volume in determining its etching behavior. By suitable choice of all the factors which influence the formation of wires, three dimensional arrays of nanoscale silicon wires can be formed, Fig. 6b. If we use more proton energies then even more rows of wires can be formed.

### Conclusions

A range of factors influence the diameter and gap between end-of-range wires in electrochemically etched p-type silicon wafers. A smaller wire diameter is typically produced with a lower line fluence and/or a lower proton energy, whereas wafer resistivity is the main factor which determines the minimum gap between adjacent wires. The location of a feature within the irradiated area is also very important in determining its resultant size. With suitable attention to these factors, both the diameter of wires and gaps between adjacent wires of 50 nm can be produced and we believe that even smaller wires and spacings are achievable using this approach. Self-aligned, three dimensional silicon nanowire arrays were also achieved. These results open a route to achieving densely-packed, three dimensional device structures for use in silicon photonics, microelectromechanical systems and for thermoelectric studies, which are difficult to fabricate

using more conventional approaches such as deep reactive ion etching or the use of silicon-on-insulator wafers.

Work partly performed at SSSL under NUS Core Support C-380-003-003-001.

### References

1. P. Polesello, C. Manfredotti, F. Fizzotti, R. Lu, E. Vittone, G. Lerondel, A. M. Rossi, G. Amato, L. Boarino, S. Galassini, M. Jaksic, and Z. Pastuovic, *Nucl. Instrum. Methods Phys. Res. B*, **158**, 173 (1999).
2. E. J. Teo, D. Mangaiyarkarasi, M. B. H. Breese, A. A. Bettioli, and D. J. Blackwood, *Appl. Phys. Lett.*, **85**, 4370 (2004).
3. M. B. H. Breese, F. J. T. Champeaux, E. J. Teo, A. A. Bettioli, and D. J. Blackwood, *Phys. Rev. B*, **73**, 035428 (2006).
4. I. Rajta, S. Z. Szilasi, P. Fürjes, Z. Fekete, and C. Dücsö, *Nucl. Instrum. Methods Phys. Res. B*, **267**, 2292 (2009).
5. F. Menzel, D. Spemann, J. Lenzner, W. Böhlmann, G. Zimmermann, and T. Butz, *Nucl. Instrum. Methods Phys. Res. B*, **267**, 2321 (2009).
6. E. J. Teo, A. A. Bettioli, P. Yang, M. B. H. Breese, B. Q. Xiong, G. Z. Mashanovich, W. R. Headley, and G. T. Reed, *Opt. Lett.*, **34**, 659 (2009).
7. D. Mangaiyarkarasi, M. B. H. Breese, Y. S. Ow, and C. Vijila, *Appl. Phys. Lett.*, **89**, 021910 (2006).
8. B. G. Svensson, B. Mohadjeri, A. Hallen, J. H. Svensson, and J. W. Corbett, *Phys. Rev. B*, **43**, 2292 (1991).
9. B. G. Svensson, C. Jagadish, A. Hallen, and J. Lalita, *Nucl. Instrum. Methods Phys. Res. B*, **106**, 183 (1995).
10. A. Hallen, N. Keskitalo, F. Masszi, and V. Nagi, *J. Appl. Phys.*, **79**, 3906 (1996).
11. M. Yamaguchi, S. J. Taylor, M. J. Yang, S. Matsuda, O. Kawasaki, and T. Hisamatsu, *J. Appl. Phys.*, **80**, 4916 (1996).
12. V. Lehmann, *Electrochemistry of Silicon: Instrumentation, Science, Materials and Applications* (Wiley-VCH, New York, 2002).
13. J. F. Ziegler, M. D. Ziegler, and J. P. Biersack, *Nucl. Instrum. Methods Phys. Res. B*, **268**, 1818 (2010).
14. J. F. Ziegler, J. P. Biersack, and U. Littmark, *The Stopping and Range of Ions in Solids* (Pergamon Press, New York, 2003).
15. P. Y. Yang, G. Z. Mashanovich, I. Gomez-Morilla, W. R. Headley, G. T. Reed, E. J. Teo, D. J. Blackwood, M. B. H. Breese, and A. A. Bettioli, *Appl. Phys. Lett.*, **90**, 241109 (2007).
16. Y. S. Ow, H. D. Liang, S. Azimi, and M. B. H. Breese, *Electrochem. Solid-State Lett.*, **14**(5), D45 (2011).
17. S. Azimi, M. B. H. Breese, Z. Y. Dang, Y. Yan, Y. S. Ow, and A. A. Bettioli, *J. Micromech. Microeng.*, **22**, 015015 (2012).
18. G. T. Reed and A. P. Knights, *Silicon Photonics: an Introduction* (John Wiley, Chichester, Hoboken, NJ, 2004).
19. D. Mangaiyarkarasi, Y. S. Ow, M. B. H. Breese, V. L. Fuh, and E. T. Xioasong, *Opt. Express*, **16**, 12757 (2008).
20. G. Léron del, R. Romestain, and S. Barret, *J. Appl. Phys.*, **81**, 6171 (1997).
21. S. Azimi, Y. S. Ow, and M. B. H. Breese, *Electrochem. Solid-State Lett.*, **13**(11), H382 (2010).
22. K. K. Lee, D. R. Lim, L. C. Kimerling, J. Shin, and F. Cerrina, *Opt. Lett.*, **26**, 1888 (2001).